A Novel High Accuracy PV Cell Model Including Self Heating and Parameter Variation

Aurel Gontean *, Septimiu Lica (ID)**, Szilard Bularka, Roland Szabo and Dan Lascu**

Applied Electronics Department, Politehnica University Timisoara, Timisoara 300006, Romania; septimiu.lica@upt.ro (S.L.); b.sziszi@yahoo.com (S.B.); roland.szabo@upt.ro (R.S.); dan.lascu@upt.ro (D.L.)
* Correspondence: aurel.gontean@upt.ro; Tel.: +40-745-121-383

Abstract: This paper proposes a novel model for a PV cell with parameters variance dependency on temperature and irradiance included. The model relies on commercial available data, calculates the cell parameters for standard conditions and then extrapolates them for the whole operating range. An up-to-date review of the PV modeling is also included with series and parallel parasitic resistance values and dependencies discussed. The parameters variance is analyzed and included in the proposed PV model, where the self-heating phenomenon is also considered. Each parameter variance is compared to the results from different authors. The model includes only standard components and can be run on any SPICE-based simulator. Unlike other approaches that consider the internal temperature as a parameter, our proposal relies on air temperature as an input and computes the actual internal temperature accordingly. Finally, the model is validated via experiments and comparisons to similar approaches are provided.

Keywords: PV cell; model; simulation; SPICE; self heating; parameters variation

1. Introduction

PV cells have been extensively studied in the last decades as solar energy is more and more accepted as a viable alternative to traditional energy sources. Rauschenbach [1] is a reference work, addressing the principles of PV energy conversion. Patel [2] covers a wider area, dealing both with wind and solar energy. The second edition of the "Handbook of Photovoltaic Science and Engineering" [3] by Luque and Hegedus is another reference book, providing rich details of all aspects regarding solar energy. Chapter 18 deals with solar cells and modules measurements and models. Aparicio et al. [4] use free software for modeling PV cells, while Sumathi et al. [5] and Khatib and Elmenreich [6] explain how to model a PV cell or array using MATLAB. Honsberg and Bowden [7] offer an online book with examples, intended for researchers and students, while in another online resource, Van Zeghbroeck [8] inspects in detail the main information of the semiconductors theory and devices. Modeling the PV behavior is useful for system design, planning, research and training. The goal of this work is to develop an accurate model for a PV cell, expandable to a whole module, using affordable tools and taking into account parameters variations. LTSpice [9] was chosen as the simulation tool due to its free cost and wide acceptance, Visual Studio Express [10], also a free tool, was used for parameters estimation and solution validation. Finally, S-Math Studio [11] was selected for the trial and error different evaluations. The solution implies a reasonable computing power and provides fast convergence. The model itself is portable, as it uses only standard components and is also vendor independent. The input data is usually provided from the manufacturer's datasheet or can be obtained via experiments.

Unlike other approaches, the model uses the ambient/air temperature and based on the irradiance it calculates the internal (silicon) temperature and provides the actual values of the parameters.

The paper is organized as follows: Section 2 briefly analyzes the classical PV model and its equations. Section 3 deals with the information provided by the PV cell datasheet and the equipment involved in measurements. Finding the solution for the PV cell model is analyzed in Section 4, with Section 4.1 introducing the solving algorithm. A review of parameters variation is the subject for Section 4.2, including the real operating conditions, when the PV solar cell is self heating. The new PV cell model is proposed in Section 4.3, the experimental results are exposed in Section 5, while conclusions are presented in Section 6.

2. The Classical PV Cell Model

The equivalent circuit of a solar cell is investigated in many prior works. It is generally accepted that a PV cell can be modeled by the circuit in Figure 1, including one [12–32], two [33–35] and rarely three or more diodes [36,37]. Erdem and Erdem [38] propose a distance learning experiment for a PV cell model using MATLAB. In [12], Green focuses on fill factor formulae. Phan and Chan [13] are among the first who provide an analytical solution for a PV model. However, they do not consider parameters variation and have a limited range for a_1. Further proposals for PV models can be found in [14,15]. Walker [16] uses a MATLAB PV model to study MPPT converter technologies. De Blas et al. [17] and Xiao et al. [18] further enhance the PV models adding new perspectives, while King et al. [19] propose a model available online using an extensive set of experimental data. De Soto et al. [20] propose a model for a PV array, while Schlosser and Ghitas [21] analyze the AC parameters of the PV cell.

Villava et al. [22] develop an accurate algorithm for finding the PV model parameters at the reference temperature. Kim et al. [23] concentrate on transient analysis based on a grid-connected PV system. Di Piazza and Vitale [24] investigate different shadowing conditions. A model dedicated to monocrystalline PV panels is proposed by Jung and Ahmed [25]; Kim and Choi [26] introduce an interesting way for finding the PV cell parameters. Advanced mathematics is used in [27] for the same purpose while Saloux et al. [28] elaborate explicit parameters finding around MPP. Further models are also proposed by Cuce [29] and Tian et al. [30].

Cubas and Pindado [31] use Lambert W-function for PV cell parameters extraction and they also provide an LTSpice model based on these parameters. In a recent paper, Aller et al. [32] propose an estimation of the PV parameters that can used in inverters power control.

Chan and Phang [33] do a pioneering work in establishing a solution for the double diode PV model with the assumption of the ideality factor being 1 for the first diode and 2 for the second diode. Sandrolini et al. [34] extract the double diode model parameters using a numerical method by cluster analysis, while Ishaque et al. [35] address the same problem using a MATLAB model, able to correctly operate also on shading conditions.

In Figure 1, I_{ph} current source models the photo generated current, with a linear dependency on the irradiance. The first diode, D_1, is associated with the diffusion mechanism. The second diode, D_2, is inserted to include the effect of charge recombination. Resistance R_s represents the cell series resistance and resistance R_{sh} the cell parallel (shunt) resistance. Resistance R_s is related to the losses in cell solder bonds, wires, junctions and so on and it is usually bellow 1 Ω. Resistance R_{sh} is related to the leakage current through the high conductivity shunts across the p-n junction and its order starts in the order of ten of ohms to several kΩ. The circuit in Figure 1 can be extended to any combination of n_s series—n_p parallel cells within a PV module (array). In this paper we shall consider only one diode in the model, D_1, neglecting D_2. The equations will be provided in a general form, while the simulations and the experiments will be conducted for a single cell, that is for $ns = np = 1$. In the remaining text, for simplicity reasons, the output cell voltage V_{ph} and the output cell current I_{ph} will be written as V and I, respectively.
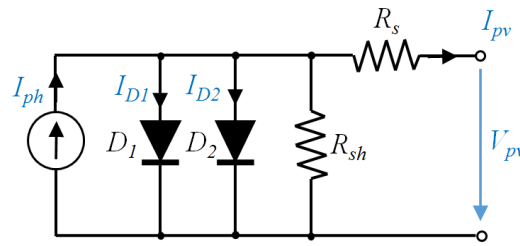
Figure 1. Equivalent circuit of a photovoltaic cell.

Referring to Figure 1, according to Kirchhoff's current law (KCL), one can write:

$$I = I_{ph} - I_{o1}\left\{\exp\left[\frac{q(V + IR_s)}{a_1 n_s kT}\right] - 1\right\} - \frac{V + IR_s}{R_{sh}} \tag{1}$$

where I_{o1} is the diode reverse saturation current, q is the electron charge, k is the Boltzmann constant, T is the actual silicon temperature and a_1 is the ideality factor of the diode.

Current I_{ph} linearly depends on irradiation and temperature [15,18]:

$$I_{ph} = \left(I_{ph,ref} + k_I \Delta T\right)\frac{G}{G_{ref}} \tag{2}$$

At the maximum power point, using (1), the maximum power P_{mp} can be derived [22]:

$$P_{mp} = V_{mp}I_{mp} = V_{mp}\left\{I_{ph} - I_{o1}\left[exp\left(\frac{q}{kT}\frac{V_{mp} + I_{mp}R_s}{a_1 n_s}\right) - 1\right] - \frac{V_{mp} + I_{mp}R_s}{R_{sh}}\right\} \tag{3}$$

Even in (1) and (3) I_{ph} is considered equal to I_{sc}, a more accurate formula for I_{ph} is [22]:

$$I_{ph,ref} = \frac{R_{sh} + R_s}{R_{sh}} I_{sc,ref} \tag{4}$$

A good overview of the PV cell performance can be found in [12], where an empirical formula for the fill factor *FF* is introduced, considering the single diode model:

$$FF = \frac{\frac{qV_{oc}}{a_1 n_s kT} - \ln\left(0.72 + \frac{qV_{oc}}{a_1 n_s kT}\right)}{\frac{qV_{oc}}{a_1 n_s kT} + 1} \tag{5}$$

3. Materials, Methods and Equipment

For our experiments we have chosen a high efficiency low cost monocrystalline Silicon PV solar cell, unmounted in panels [39]. The datasheet of the PV cell offers a limited amount of data, summarized in Table 1.

Table 1. PV Cell main specifications on STC (1000 W/m^2, AM 1.5, 25 °C).

Symbol	Description	Value
$V_{oc,cell,ref}$	Cell open circuit voltage	0.699 V
$I_{sc,ref}$	Short circuit current	9.206 A
V_{mp}	Maximum power voltage	0.572 V
I_{mp}	Maximum power current	8.756 A
(P_{mp})	Maximum power $P_{mp} = V_{mp}I_{mp}$	(5.21 W)
FF	Fill factor	(81.90%)
k_I	Short circuit temperature coefficient	0.035 %/K
k_V	Open circuit voltage temperature coefficient	−0.25 %/K
k_P	Maximum power temperature coefficient	−0.41 %/K

It is important to note that $V_{mp} = (0.75, \ldots, 0.9)V_{oc}$ for any solar cell. This is a good starting point for any simulation or MPPT algorithm implementation.

The data from the datasheet is confusing, as:

1. The claimed maximum power (5.21 W) differs from $V_{mp}I_{mp} = 5.01$ W. This latter value will be considered subsequently.

2. The claimed fill factor (81.90%) differs from the standard definition $FF = \frac{V_{mp}I_{mp}}{V_{oc,ref}I_{oc,ref}} = 77.82\%$.

The empirical Equation (5) yields an approximate result ($FF \cong 84.08\%$) when compared to the datasheet values (Table 1).

The irradiance was measured with a Klipp and Zonen SHP1 pyrheliometer with integrated temperature sensor for temperature compensation. The internal silicon temperature was determined with a FLIR E8 infrared camera and a PT1000 temperature sensor on the rear of the PV cell. In order to obtain reliable data, the PT1000 temperature sensor was glued with high thermally conductive adhesive to the backside metal coating of the PV cell. The ambient temperature was measured using the National Instruments NI USB T01 interface. Due to the extremely low internal series resistance R_s, several series cells were carefully wired and a Kelvin connection had to be used for voltage measurements. The measurements were performed under real life conditions, when the solar irradiance was maximum with the PV cells oriented toward the sun on 45 degree inclined support. The load was an ET Instrument ESL-Solar, configured in MPPT mode.

The accuracy of the irradiance measurement relies on the Klipp and Zonen SHP1 pyrheliometer with zero offset due to temperature change, temperature dependence of sensitivity below 0.5% from -30 to $+60$ °C and nonlinearity below 0.2% for up to 1000 W/m^2 irradiance. The accuracy of the temperature sensor for the ambient temperature and PV cell backside coating is 0.6 °C in the measurement range of 0–60 °C. The FLIR E8 infrared camera has an accuracy of 2 °C with thermal sensitivity below 0.06 °C. The accuracy of the FLIR infrared camera is lower than the measurements taken with the temperature sensors but offers the advantage of contactless measurement which is important for PV cell front side measurements. However, the existence of hot spots can be easily observed with this method. The electrical noise was minimized using the following digital busses for communication: Modbus for irradiance and PV cell back side temperature measurement, USB for ambient and PV cell front side temperature measurements.

4. Classical Model Solving

Several ways for solving the equations have been proposed. In [17] de Blas et al. assume the operation of a solar module at high irradiance levels and deduce the parameters accordingly. De Soto et al. [20] show how the values of parameters for the five-parameter model can be determined for four different cell technologies. The methods introduced in [22,26] are somehow similar, the parameters being precisely extracted by letting the resistance values converge to the actual value in repeated numerical loop computations. Ishaque and Salam [27] use the differential evolution for parameters extraction. Saloux et al. [28] introduce a model able to predict the short-circuit current, the open-circuit voltage and the maximum cell power. Tian et al. [30] concentrate on an extension of the PV cell model for modules and arrays, for monocrystalline and polycrystalline silicon, used for shading effect investigation under different operating conditions.

One of the difficulties is the implicit nature of Equation (1) regarding I. This has been addressed by various techniques, ranging from pure mathematical approaches (including Lambertian W-Function, [31]) to pure numerical solutions, mainly in MATLAB [5,6,16,35].

Later models take into account the parameters variation with temperature and irradiance. Radziemska and Klugmann [40] analyze the temperature influence on the I-V curves of the PV cell, while Tsuno et al. [41] include also the irradiance in the analysis. Singh et al. [42] also present the temperature influence, while Cuce and Bali [43] focus on parameters variation in humid climates. The Lambert W-function is again used by Ghani and Duke [44] to estimate the parasitic resistances

of the PV cell. The correlation between the temperature and PV cell efficiency is addressed in [45,46]. Temperature and irradiance influence on the PV cell characteristics via experiments is presented in [47,48]. Araneo et al. [49] propose a model to predict the PV cell temperature based on date, time and geographical position. Temperature and irradiance influence are also investigated in two recent papers by Chander et al. [50] and Aller et al. [51]. However the most common approach considers the internal PV temperature as an independent parameter and plots the I-V family curves for different temperatures. This aspect will be covered in the subsequent sections. It has to be stressed out that the exponential nature of Equation (1) determines that a small variation in any of the terms involved in the exponential term to substantially modify the final result. This aspect will be addressed in Sections 5 and 6.

4.1. Solving the Equations for the Classical PV Model

The method introduced here is an extension of the method proposed by Villalva et al. [22] and involves the following steps:

1. Compute a_1
2. For validation purposes determine the limits $R_{s,max}$ and $R_{sh,min}$
3. For all values between $[0, R_{s,max}]$ with $R_{s,inc}$ as increment, numerically solve (1) for the MPP.
4. When the maximum power error is below the imposed threshold error, R_s is established and R_{sh} can be computed.

A VB.net application has been developed by the authors in order to numerically solve and compute the model parameters. The application can be downloaded from http://tess.upt.ro. Figure 2 depicts a print screen for the initial parameter passing (a) and the results (b).

(**a**)   (**b**)
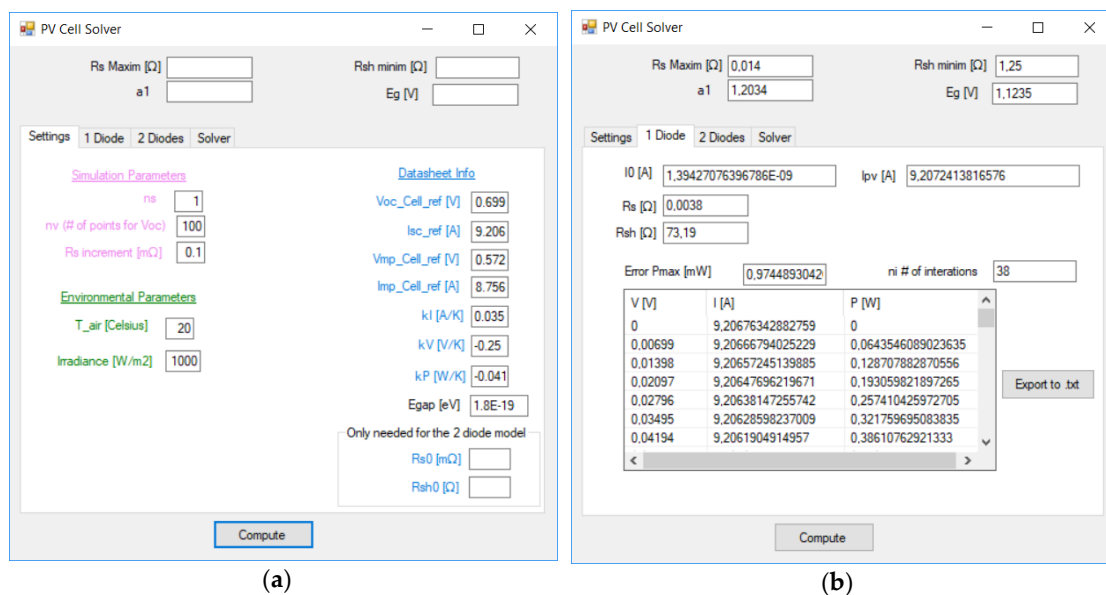
Figure 2. VB.net PV Cell solver: (**a**) Entering parameters values; (**b**) getting the solution.

In our case, using the values taken from the datasheet for $n_s = n_p = 1$, it results that:

$$R_{s,max} = \frac{V_{oc} - V_{mp}}{I_{mp}} = 14 \text{ m}\Omega \tag{6}$$

$$R_{p,min} = \frac{V_{mp}}{I_{sc,ref} - I_{mp}} - R_{s,max} = 1.25 \ \Omega \tag{7}$$

These limits are important to set reliable ranges for the algorithm. The final results are listed in Table 2.

Table 2. Vb.net application results.

Symbol	Description	Results
$I_{ph,ref}$	Photo generated current	9.207 A
$I_{o,ref}$	Reverse diode current	1.39427 nA
$R_{s,max}$	Maximum R_s value (initial guess)	14 mΩ
$R_{s,ref}$	Series resistance	3.8 mΩ
$R_{sh,min}$	Minimum R_{sh} value (initial guess)	1.25 Ω
$R_{sh,ref}$	Parallel resistance	73.19 Ω
$a_{1,ref}$	Ideality factor	1.2034
$E_{g,ref}$	Bandgap energy	1.795×10^{-9} V
$V_{g,ref}$	Bandgap voltage	1.121 V

Several attempts have been made for finding explicit expressions for R_s and R_{sh} based on actual datasheet data. For example, Cubas et al. [31] offer the R_{sh} formula (with R_s as an argument, considering $n_s = 1$):

$$R_{sh} = \frac{\left(V_{mp} - I_{mp}R_s\right)\left[V_{mp} - R_s\left(I_{sc} - I_{mp}\right) - \frac{a_1 kT}{q}\right]}{\left(V_{mp} - I_{mp}R_s\right)\left(I_{sc} - I_{mp}\right) - \frac{a_1 kT I_{mp}}{q}} \tag{8}$$

For the above data, the R_{sh} formula (8) yields a result of 59.43 Ω, compared to the actual value of 73.19 Ω.

In a simplified model ($R_{sh} \to \infty$), Xiao et al. [18] propose for R_s the following relationship (again $n_s = 1$):

$$R_s = \frac{\frac{a_1 kT}{q} ln\left[\left(1 - \frac{I_{mp}}{I_{ph}}\right)exp\left(\frac{qV_{oc}}{a_1 kT}\right) + \frac{I_{mp}}{I_{ph}}\right] - V_{mp}}{I_{mp}} \tag{9}$$

Here (9) yields $R_s = 0.7$ mΩ, quite far from its actual value (3.8 mΩ).

4.2. Parameters Variation for Different Conditions

The parameters in Equations (1)–(4) are not constant over the environmental conditions, as $I_o, R_s, R_{sh}, a_i, E_g$ depend on temperature and irradiance. A brief review of these dependencies is provided bellow.

4.2.1. Diode Saturation Current—I_{o1}

Phang et al. [13] show that if I_{pv} is below 10 A, I_{o1} can be derived as in (10):

$$I_{o1} = \left(I_{sc} - \frac{V_{oc}}{R_{sh}}\right)exp\left(-\frac{V_{oc}}{a_1 V_T}\right) \tag{10}$$

I_{o1} in (10) yields a very good result of 1.3969 nA vs. 1.39427 nA obtained in Table 2. Gow and Manning [15] were among the first to claim that:

$$I_{o1} = C_1 T^3 e^{-\frac{qV_g}{kT}} \tag{11}$$

The temperature dependence of this current is more detailed expressed by [16,20]:

$$I_{o1} = I_{o1,ref}\left(\frac{T}{T_{25}}\right)^3 exp\left[\frac{qV_g}{ka_1}\left(\frac{1}{T_{ref}} - \frac{1}{T}\right)\right] \tag{12}$$

where V_g is the bandgap voltage of the semiconductor ($V_g = 1.1, \ldots, 1.3$ V for Si at 25 °C).

$I_{o1,ref}$ can be derived from (1) at the reference temperature as:

$$I_{o1,ref} = \frac{I_{sc,ref}}{\exp\left(\frac{qV_{oc,ref}}{a_1 n_s k T_{ref}}\right) - 1} \tag{13}$$

According to Vilalva et al. [22], $I_{o1,ref}$ can be further improved:

$$I_{o1,ref} = \frac{I_{sc,ref} + k_I \Delta T}{\exp\left[\frac{q(V_{oc,ref} + k_V \Delta T)}{a_1 n_s k T}\right] - 1} \tag{14}$$

In subchapter 4.6.3 of [8], Van Zeghbroeck states an equation in which $I_{o1,ref}$ can be derived from, that can offer an alternate way to estimate $I_{o1,ref}$:

$$V_{mp} = V_{mp} \ln \frac{1 + \frac{I_{ph}}{I_{o1,ref}}}{1 + \frac{V_{mp}}{V_T}} \tag{15}$$

This proves to be not very accurate in our case, as with the values from Table 1, $I_{o,ref}$ from (15) results 0.085 nA, quite far from the actual value (1.39427 nA).

4.2.2. Band Gap Energy and Bandgap Voltage—E_g, V_g

Van Zeghbroeck [8] shows that the bandgap energy, E_g, exhibits a small temperature dependence as in (16).

$$E_g = 1.166 - \frac{0.000477 T^2}{636 + T} \tag{16}$$

From (16), $E_{g,ref} = 1.121$ eV for silicon cells at 25 °C. This is the value considered in Table 1.
In contrast, Kim et al. [23] define the variance for E_g for silicon to be:

$$E_g = 1.16 - \frac{7.02 \times 10^{-4} T^2}{T - 1108} \tag{17}$$

Both (16) and (17) fit in the [1.1, ... , 1.3] V interval specified when Equation (12) was introduced. In our approach shown in Figure 3, we adopted the Van Zeghbroeck proposal because it will finally lead to a more realistic value for a_1 and close to the linear approximation of E_g against temperature suggested by Radziemska and Klugmann [40], which indicate a temperature coefficient $dE_g/dT = -2.3 \times 10^{-4}$eV/K.
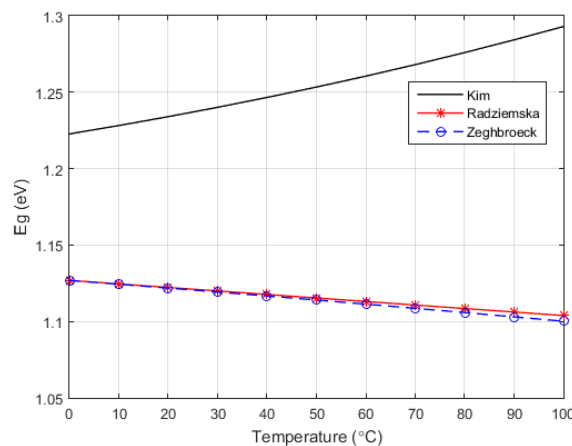
Figure 3. E_g variation against temperature according to several authors.

4.2.3. Series Resistance—R_s

Honsberg and Bowden [7] show that R_s does not influence V_{oc}, but close to the open-circuit voltage, the I-V curve is affected by R_s. An initial estimation for R_s is to find the slope of the I-V curve at the open-circuit voltage point (18):

$$R_{so} = -\left.\frac{dV}{dI}\right|_{V=V_{oc}} \tag{18}$$

In our case, $R_{so} = 11$ mΩ (while $R_s = 3.8$ mΩ, as it will later be shown).

Cuce and Bali [43], Cuce et al. [47] and Singh et al. [42] claim that R_s linearly decreases with the temperature. Obviously, reducing R_s yields an increase in the output current.

A PV Cell model is also available in MATLAB Simscape [52]. It consists of the same circuit as in Figure 1, where the user can choose between:

- An 8-parameter model, where Equation (1) describes the output current
- A 5-parameter model that neglects D_2 in Figure 1 and the value of the shunt resistor is infinite.

Both models adjust the resistance values and current parameters as a function of temperature. Resistance R_s is assumed to be given by (19):

$$R_s = R_{s,ref}\left(\frac{T}{T_{ref}}\right)^{k'_{Rs}} \tag{19}$$

where k'_{Rs} is the temperature exponent for R_s. k'_{Rs} is 0 by default and when modified has to be positive.

Figure 4 summarizes all these above dependencies. In order to have the results in the same range, Cubas et al. [31] and Cuce et al. [47] results were scaled, and Equation (19) was re-written as in (20), interchanging T with T_{ref} and k_{Rs} was estimated as 4.9 for the best fit. A linear dependency is easy to implement, but might also lead to results not physically true (for example Cuce et al. [47] data lead to negative R_s resistances for temperatures over 75 °C and so does Cubas et al. [31] over 97 °C).

$$R_s = R_{s,ref}\left(\frac{T_{ref}}{T}\right)^{k_{Rs}} \tag{20}$$

where $|k'_{Rs}| = |k_{Rs}|$.
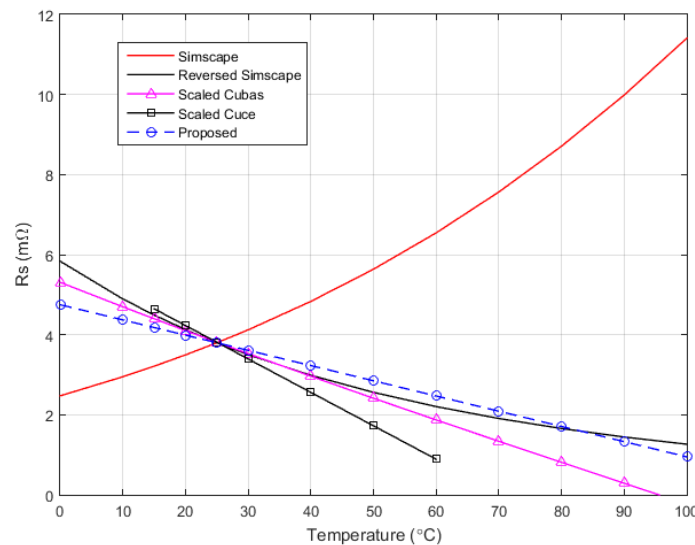
Figure 4. R_s variation against temperature by several authors.

The linear law (21) was adopted for R_s and we chose $\alpha_{Rs} = -0.01\ \text{K}^{-1}$, again for the best fit.

$$R_s = R_{s,ref}\left[1 + \alpha_{Rs}\left(T - T_{ref}\right)\right] \tag{21}$$

4.2.4. Parallel Resistance—R_{sh}

Honsberg and Bowden [7] and Jung and Ahmed [25] showed that the shunt resistance of a solar cell can be determined from the slope of the I-V curve close to the short-circuit point, yielding a fair approximation for R_{sh}:

$$R_{sho} = -\left.\frac{dV}{dI}\right|_{I=I_{sc}} \tag{22}$$

From our experimental data, $R_{sho} = 73.18\ \Omega$, very close to the accurate solution $R_{sh} = 73.19\ \Omega$, as it will later be illustrated.

Cuce and Bali [43] and Cuce et al. [47] claim that the shunt resistance linearly decreases with temperature. They explain this decrease in terms of a combination of tunneling and trapping–detrapping of the carriers through the defect states in the space-charge region of the device. These defect states act either as recombination centers or as traps depending upon the relative capture cross sections of the electrons and holes for the defect. Temperature dependency for R_{sh} is however more complicate.

R_{sh} is again modeled in MATLAB Simscape like (23):

$$R_{sh} = R_{sh,ref}\left(\frac{T}{T_{ref}}\right)^{k'_{Rsh}} \tag{23}$$

where k'_{Rsh} is the temperature exponent for R_{sh}. k'_{Rsh} is 0 by default and when modified has to be positive.

Figure 5 summarizes all these R_{sh} equations. In order to bring the results in the same range, Cubas et al. [31] and Cuce et al. [47] dependencies were scaled, and Equation (23) was re-written as in (24) interchanging T with T_{ref} and k_{Rsh} was estimated as 8 for best fit.

$$R_{sh} = R_{sh,ref}\left(\frac{T_{ref}}{T}\right)^{k_{Rsh}} \tag{24}$$

where $\left|k'_{Rsh}\right| = \left|k_{Rsh}\right|$.
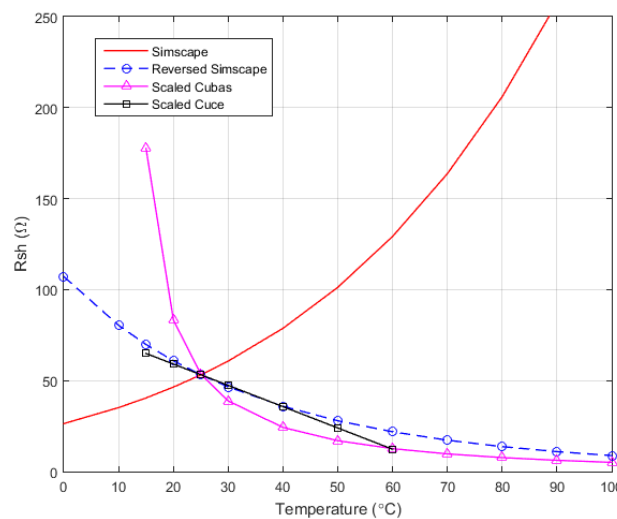
Figure 5. R_{sh} variation over temperature by several authors.

Although R_{sh} influence is small in the overall model, for an accurate modeling and especially for larger temperature ranges R_{sh} linear variation is not realistic. Therefore in our model described by (24) we chose $k_{Rsh} = 8$.

4.2.5. Ideality Diode Factor—a_1

Some authors consider the ideality factor as being constant over the operating temperature range and with a generic value for a_1 in the interval [1, 1.5] for every kind of cell [22,31]. Cuce et al. [29] propose $a_1 = 1.2$ for monocrystalline silicon cells, and $a_1 = 1.3$ for polycrystalline ones. Some studies indicate a linear decreasing with temperature [18]. Cubas et al. [31] say that "the lack of accuracy produced when considering the ideality factor as constant is generally reduced, given that variations of this parameter only affects the curvature of the I-V curve." This is arguable, as a_1 interferes in an exponential dependency and small variations of a_1 lead to significant changes in I_{01}, and finally in I. One might say that picking a random a_1 in the above specified range will be balanced by a different I_o, so only the pair (I_o, a_1) matters. However this approach is misleading, as it may induce impossible physical solutions.

Phang et al. [13] have the following proposal:

$$a_1 = \frac{q\left(V_{mp} + I_{mp}R_{so} - V_{oc}\right)}{kT_{ref}\left[ln\left(\frac{I_{sc} - \frac{V_{mp}}{R_{sho}} - I_{mp}}{I_{sc} - \frac{V_{oc}}{R_{sh}}}\right) + \frac{I_{mp}}{I_{sc} - \frac{V_{oc}}{R_{sho}}}\right]} \tag{25}$$

De Blas et al. [17] suggest that:

$$a_1 = \frac{q\left(V_{mp} + I_{mp}R_s - V_{oc}\right)}{kT_{ref}ln\left[\frac{I_{sc} - I_{mp}\left(1 + \frac{R_s}{R_{sh}}\right) - \frac{V_{mp}}{R_{sh}}}{I_{sc}\left(1 + \frac{R_s}{R_{sh}}\right) - \frac{V_{oc}}{R_{sh}}}\right]} \tag{26}$$

E. Saloux et al. [28] somehow simplify (26) as below:

$$a_1 = \frac{q\left(V_{mp} - V_{oc}\right)}{kT_{ref}ln\left(1 - \frac{I_{mp}}{I_{sc}}\right)} \tag{27}$$

In the algorithm of Villalva [53], a different formula is introduced. Considering that for crystalline silicon $E_g = 1.8$ J, V_g becomes 1.1235 V and the following formula provides a good result (Formula (28) was adapted from [53], as the additional presence of the n_s in the initial formula provided correct results only for $n_s = 1$), thus eliminating a trial and error time consuming for the initial guess of a_1:

$$a_1 = \frac{q\left(k_V - \frac{V_{oc}}{n_s T_{ref}}\right)}{kT_{ref}\left(\frac{k_I}{I_{ph}} - \frac{3}{T_{ref}} - \frac{E_g}{kT_{ref}^2}\right)} \tag{28}$$

The results for a_1 are summarized in Table 3, with a very good correlation between (25), (26) and (28). This is the reason we have adopted the Villalva value of 1.2034.

Table 3. Different a_1 values.

a_1 Accepted Range	Phang, Equation (25)	De Blas, Equation (26)	Saloux, Equation (27)	Villalva, Equation (28)
1–1.5	1.1952	1.2016	1.6377	1.2034

Xiao et al. [18] specify a linear decreases of the ideality factor with the temperature for the Shell ST40 module, ranging from 1.85 to 1.15, corresponding to 5 to 45 Celsius degree variance respectively. From the data plotted in their work, the following law can be adopted:

$$a_1 = 7.013 - 0.01875T \tag{29}$$

Such approach must be taken with extreme care, as it is a common practice to operate often at temperatures higher than 48 °C, where (29) yields $a_1 = 1$ (or 0 at 100 °C)

De Soto et al. [20] come with a different proposal:

$$a_1 = a'_{1,ref} \frac{T}{T_{ref}} \tag{30}$$

which has a wrong slope. For a proper variation T and T_{ref} should be reversed as follows:

$$a_1 = a_{1,ref} \frac{T_{ref}}{T} \tag{31}$$

Our experiments presented in Figure 6 yielded a different result, closer to reversed Soto (31), according to the following linear dependency:

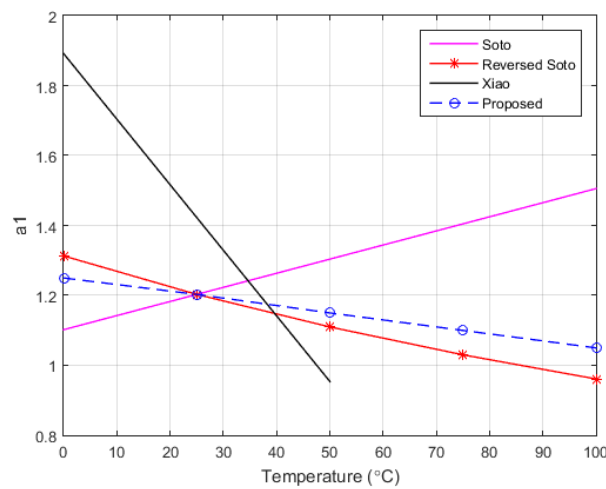$$a_1 = 1.2512 - 0.002(T - 273.15) \tag{32}$$

Figure 6. a_1 vs. temperature.

4.2.6. Self Heating Phenomenon

It is a common practice to express the internal cell temperature, T_{cell} based on Normal Operating Cell Temperature (NOCT) data, when the module is mounted 45° from horizontal.

$$T_{cell} = T_{amb} + (NOCT - 20) \frac{G}{800} \tag{33}$$

Here $G = 800 \text{ W/m}^2$, $T_{amb} = 20 \text{ °C}$ and airflow is 1 m/s [45].

The internal temperature of the PV was of permanent concern for the researchers [40–42,46], but in most situations just an uncorrelated dependency is studied. Simply the temperature dependency of the I-V characteristic without acknowledging neither the real, actual temperature of the PV nor parameter variation is considered. Advanced simulators software packages include such features, MATLAB Simscape [52] being one of them.

In a recent work, Krac and Górecki [54] introduced a thermal model for the PV cell, where the self heating is modeled. The thermal behavior is modeled by a thermal resistor and a thermal capacitor, a voltage source related to the ambient temperature and a current source that represents the total dissipated power within the PV. They claim that "for the maximum allowable value of the panel forward current (equal to 8 A), a self heating phenomenon causes an increase in the panel temperature value equal only by 12 °C." In our experiments, we acquired a rather extended influence, ranging from 20 to 30 °C.

Opposite to [55,56], the power dissipated by the PV cell is taken into account from the dissipative elements, which are resistive in our model. The energy flows from the two current sources to the resistors and the external circuit. Two or three current sources (or even diodes) are used in order to model different phenomena that take place inside the PV cell, the photoelectric effect and the behavior of p-n junction [8].

4.2.7. Open Circuit Voltage—V_{oc}

Ishaque and Salam [27] propose for the $V_{oc,cell}$ the following variation (34), which proves good correlation with the datasheet info and experimental data—see also Figure 7:

$$V_{oc,cell} = V_{oc,cell,ref} + a_1\frac{kT}{q}ln\frac{G}{G_{ref}} + k_v\Delta T \tag{34}$$
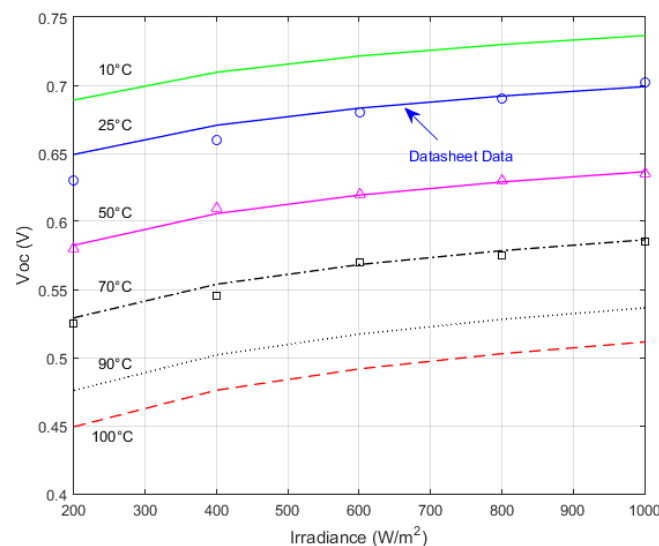
Figure 7. $V_{oc,cell}$ vs. Irradiance for different temperatures. Solid and dashed lines are given by (33), while symbols correspond to experimental data.

Even (34) is not necessary for the model, it is another starting point for computing a_1.

4.3. The New Proposed PV Cell Model

The proposed model is presented in Figure 8. The upper section consists of standard elements, while the thermal modeling is ensured by the lower section. Here the current source labeled P_d simulates the power dissipated in the cell, the voltage labeled T_j is the cell temperature and the air temperature is modeled by the voltage source T_{amb}. The thermal resistance R_{th} models the thermal flow through the system structure, in our case the PV cell. The thermal capacitance C_{th} models the thermal inertia of the PV cell. Both R_{th} and C_{th} emulate all thermal transmission phenomena (conduction, convection and radiation) and depend of the materials, the finishing of the surfaces and on the mechanical dimensions of the system.

The practical LTSpice model implementation is depicted in Figure 9 and can be found at http://tess.upt.ro. The upper circuit addresses the standard conditions (for reference and validation), while the middle section deals with the thermal model of the PV solar cell. The power associated with the circuit also includes the power due to the irradiance scaled with the cell area and the electrical power dissipated in R_s and R_{sh}.
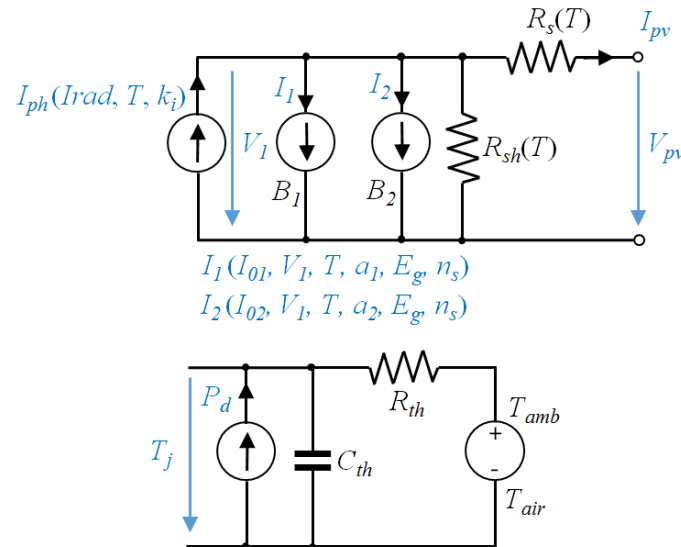

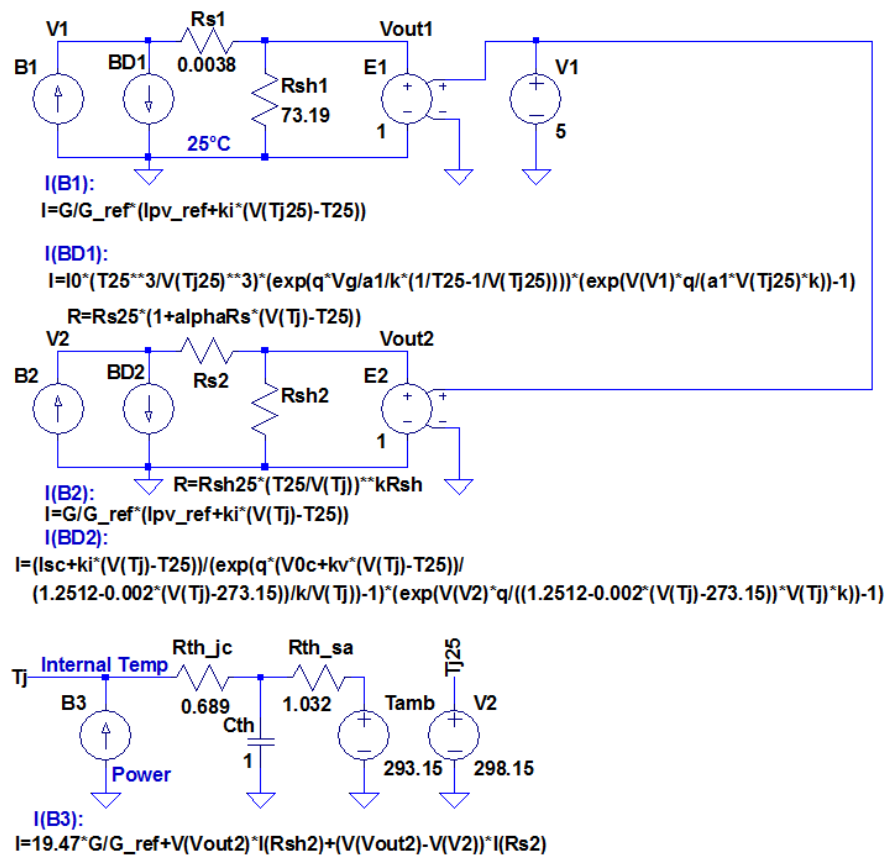**Figure 8.** The new proposed electrical and thermal model of the PV cell.

Figure 9. LTSpice PV Cell proposed model.

The thermal parameters R_{th} and C_{th} were extracted from experimental data, similar to [54]. After a set of data was acquired, the temperature against time curve variation was fit and the time constant and the steady state value were determined. Unlike Górecki and Krac [55,56], we considered no dissipated power occurs in the BD2 current source of the model in Figure 9, as it makes no physical sense.

5. Experimental Results

Figure 10 exhibits the simulated and the measured internal temperature of the PV cell and the dissipated power variation. It is worth mentioning that the corresponding NOCT for the temperature in Figure 9 is 47.2 °C.
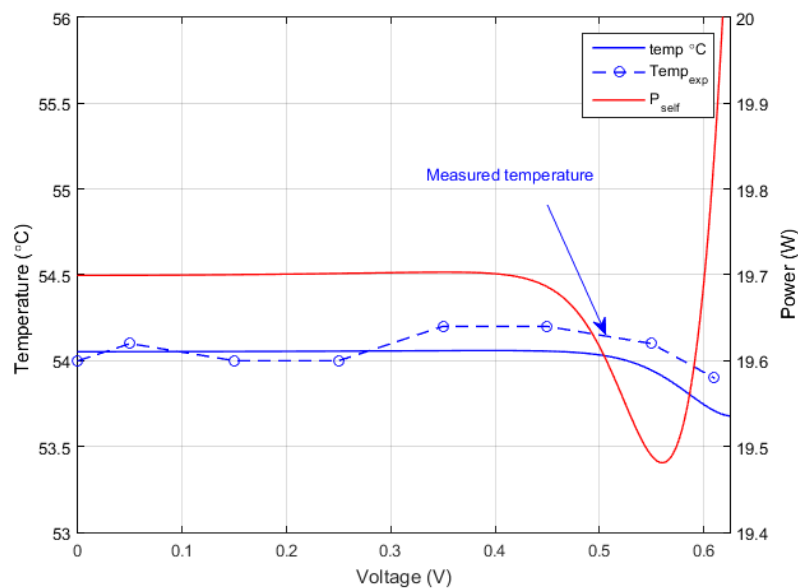

Figure 10. PV Cell dissipated power and temperature variation against voltage at STC.

Table 4 summarizes the main results for both the proposed model and the experiments performed for the PV cell. It can be observed that perfect agreement between the simulated and measured results is achieved.

Table 4. Comparison of the results at STC (25 Celsius, 1000 W/m^2).

| Symbol	Description	Datasheet Value	Proposed Model	Model Error vs. Datasheet (%)	Experimental Values	
					Results	Error vs. Datasheet (%)
$V_{oc,cell,ref}$	Cell open circuit voltage	0.699 V	0.6985 V	−0.07%	0.693 V	−0.86
$I_{sc,ref}$	Short circuit current	9.206 A	9.206 A	0%	9.221 A	0.16
V_{mp}	Maximum power voltage	0.572 V	0.575 V	0.52%	0.569 V	−0.52
I_{mp}	Maximum power current	8.756 A	8.705 A	−0.58%	8.731 A	−0.29
(P_{mp})	Maximum power $P_{mp} = V_{mp}I_{mp}$	5.01 W	5.005 W	−0.06%	4.968 W	−0.81
FF	Fill factor	77.83%	77.84%	0.01%	77.52%	−0.40

The final validation of the model is presented in Figures 11 and 12. Here the I-V and P-V characteristics of the PV cell are plotted at the reference temperature and at the operating temperature.

Experimental data is represented with markers while the lines correspond to simulated results with the model proposed. A good correlation between the model and the experiments can be noticed.

Figure 12a displays the serial resistance R_s influence on the output current and power. The solid lines graphs correspond to a fixed R_s while the dashed lines correspond to variable R_s with all the parameters included. At MPP a 98 mW power increase was observed. As estimated before, R_{sh} has a minor influence on the PV output—only 4.6 mW power decrease at MPP could be noticed, as displayed in Figure 12b. It is worth mentioning that in all cases the model self-computes the appropriate values for R_s and R_{sh} based on the predicted internal temperature.
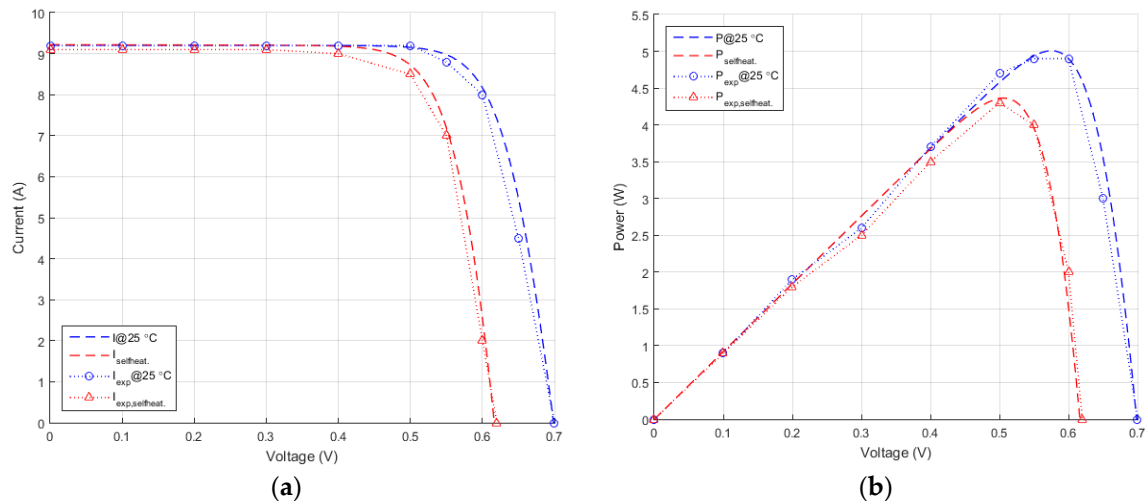
Figure 11. I-V and P-V curves—simulation and experiments. (**a**) I-V curves at 25 °C (upper lines) and with all parameters variation included (lower lines)—internal temperature is 54 °C. (**b**) P-V curves at 25 °C (upper lines) and with all parameters variation included (lower lines)—internal temperature is 54 °C.
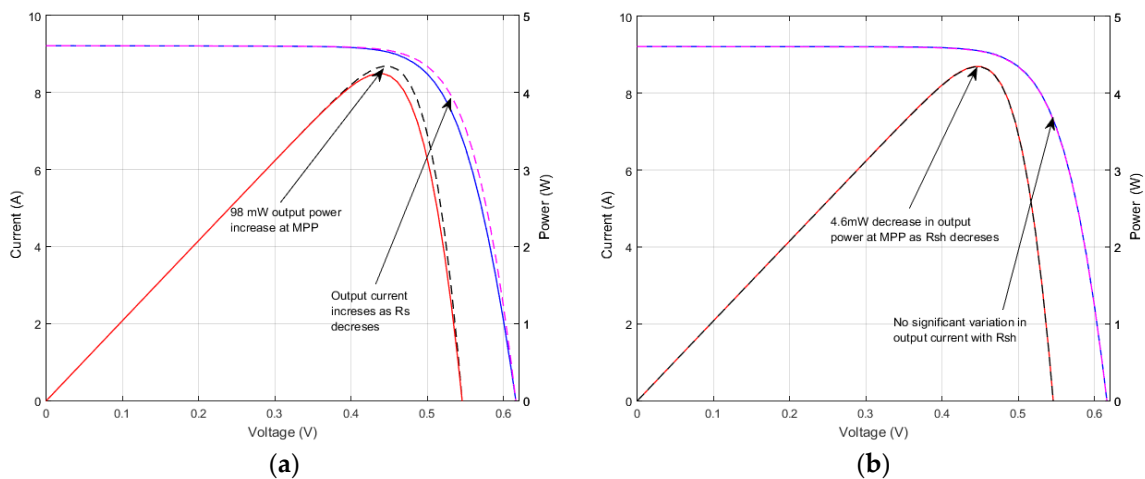
Figure 12. R_s and R_{sh} influence and the performance. (**a**) R_s increase with temperature (25 °C to 54 °C) determines an increase in the output current and power (**b**) R_{sh} has no significant influence on the performance.

PV arrays compared (Table 5) were monocrystalline (Shell SP-70, MSMD290AS-36.EU and multycrystaline (Kyocera KG200GT, MSP300AS-36.EU, MSP290AS-36.EU, Sharp ND-224uC1).

All the data from Table 5 was processed with the above proposed algorithm and the results are listed in Table 6, along with similar results from other researchers.

**Table 5.** Datasheet available information for several commercial PV arrays.

PV Type	n_s	V_{oc} (V)	V_{mp} (V)	I_{mp} (A)	I_{sc} (A)	k_V (mV/K)	k_I (mA/K)
Shell SP-70	36	21.4	16.5	4.24	4.7	−76	2
MSMD290AS-36.EU	72	44.68	37.66	7.7	8.24	−138.508	3.296
MSP290AS-36.EU	72	44.32	37.08	7.82	8.37	−146.256	3.348
KG200GT	54	32.9	26.3	7.61	8.21	−123	3.18
Sharp ND-224uC1	60	36.6	29.3	7.66	8.33	−131.76	4.4149

**Table 6.** Comparison between previous solutions and our proposed model.

PV Type	Solution	a_1	R_s (mΩ)	R_{sh} (Ω)	I_{pv} (A)	I_o (nA)
Shell SP-70	Ishaque * [35]	1 & 2.2	510	91	4.7	0.421; 0.421
	Proposed	1.022	505	73.85	4.732	0.657
MSMD290AS-36.EU	Cubas [31]	1.1	130	316	8.24	2.36
	Proposed	1.0	159	194	8.247	0.243
MSP290AS-36.EU	Cubas [31]	1.1	162	331	8.37	2.86
	Proposed	1.02	191	230	8.377	0.513
KG200GT	Ishaque * [35]	1 & 2.2	320	160.5	8.21	0.422; 0.422
	Sumathi et al. [5]	1.3	221	415.4	8.214	98.25
	Proposed	1.08	305	186	8.223	2.15
Sharp ND-224uC1	Proposed	1.06	316	108	8.354	1.41

* Ishaque et al. [35] use a 2 diode model with equal saturation currents.

The final validation of the model was by applying the introduced model and computation method for the MSMD290AS-36.EU monocrystalline PV cell array and compare the results to the ones provided by Cubas et al. [31], as shown in Figure 13. As it can be seen, a good correlation exists between the two approaches.

(a)

(b)
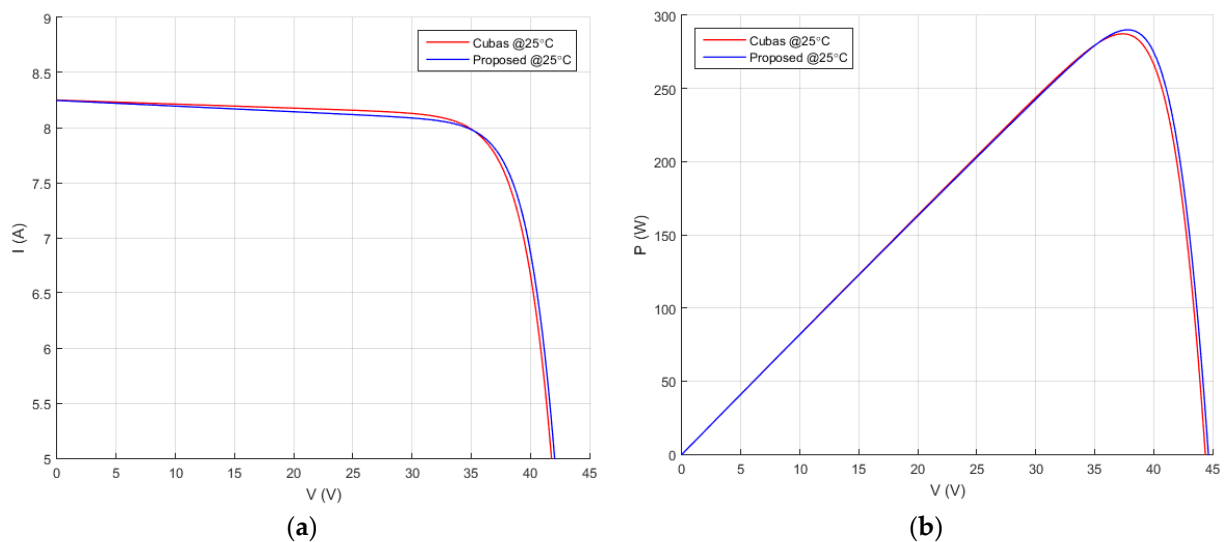
Figure 13. *Cont.*
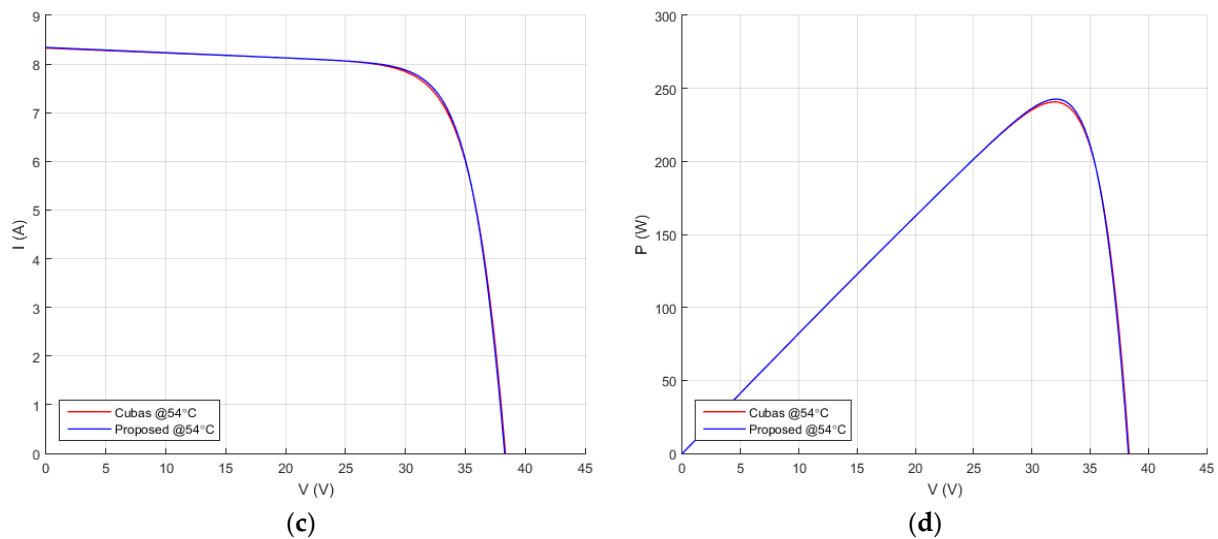
Figure 13. Final model validation by comparison for the MSMD290AS-36.EU monocrystalline PV cells. (**a**) I-V curves at 25 °C; (**b**) P-V curves at 25 °C (**c**) I-V curves at 54 °C (**d**) P-V curves at 54 °C.

6. Conclusions

A new thermo-electrical model for the PV cell was introduced. Only free available tools were used during modeling. The literature analysis proved discrepancies between authors when studying parameters variation and a more precise model is proposed in this paper.

The model proved to be accurate, while considering parameter variation and selfheating phenomenon. To the best of our knowledge this is the first time when all these parameters are included in a PV model. The internal silicon operating temperature at 1 Sun (with the ambient temperature being 20 °C) is 54 °C predicted by our model and validated by measurements performed with the FLIR and the PT1000 sensors.

As other authors have mentioned, R_{sh} influence is relatively reduced in the model. However a_1 proved to be a major factor. E_g displayed a small variance with temperature. Resistance R_s influence is important but sometimes shadowed by the wiring. The proposed model was accurately confirmed and validated by the experiments.

Author Contributions: All of the authors have contributed to this research. Aurel Gontean conceived and designed the study. Aurel Gontean and Septimiu Lica carried out the simulation. Szilard Bularka performed the experiments. Dan Lascu analyzed the data. Aurel Gontean wrote the paper. Dan Lascu reviewed the manuscript. All authors read and approved the manuscript.

Conflicts of Interest: The authors declare no conflict of interest.

Nomenclature

Main Symbols

a_1	Diode ideality factor
$a_{1,ref}$	Diode ideality factor at 25 °C
R_{th}	Thermal capacitance of the cell, a lumped parameter
E_g	Bandgap energy
FF	Fill factor
G	Actual irradiance on cell surface
G_{ref}	Reference irradiance, 1000 W/m^2
I	Solar cell current
I_{o1}	Saturation current of the modeled diode, due to diffusion

$I_{o1,ref}$	Saturation current of the modeled diode, due to diffusion, at 25 °C
I_{mp}	Current at maximum power point
I_{ph}	Photo generated current
$I_{ph,ref}$	Photo generated reference current at 25 °C
I_{sc}	Short circuit current of the solar cell
$I_{sc,ref}$	Short circuit current of the solar cell at 25 °C
k	Boltzmann constant
k_I	Current temperature coefficient, A/K
k_V	Voltage temperature coefficient, V/K
k_P	Power temperature coefficient, W/K
$k_{R_s}, k_{R_{sh}}$	R_s, R_{sh} temperature exponent
k'_{Rs}, k'_{Rsh}	R_s, R_{sh} temperature exponent in Matlab
n_s	Number of series cells
n_p	Number of parallel cells
$P_{mp} = V_{mp} I_{mp}$	Maximum power
q	Electron charge
R_s	Cell series resistance
$R_{s,ref}$	Cell series resistance at 25 °C
R_{so}	Cell series resistance based on slope close to V_{oc}
R_{sh}	Cell parallel (shunt) resistance
$R_{sh,ref}$	Cell parallel (shunt) resistance, at 25 °C
R_{sho}	Cell parallel (shunt) resistance based on slope close to I_{sc}
R_{th}	Thermal resistance of the cell, a lumped parameter
T	Solar cell temperature, K
$T_{ref} = T_{25}$	Reference temperature 298 K
$\Delta T = T - T_{ref}$	Temperature difference
T_{amb}	Ambient/air temperature, °C
T_{cell}	Internal PV cell temperature, °C
V	Solar cell voltage
V_{oc}	Solar array open circuit voltage
$V_{oc,ref}$	Solar array open circuit reference voltage at 25 °C
$V_{oc,cell}$	Solar cell open circuit voltage
$V_{oc,cell,ref}$	Solar cell open circuit reference voltage at 25 °C
V_{mp}	Voltage at maximum power point
V_g	Bandgap voltage
$V_T = kT/q$	Diode thermal voltage

Abbreviations

AM	Air Mass
KCL	Kirchhoff's current law
MPP	Maximum power point
MPPT	Maximum Power Point Tracking
NOCT	Normal Operating Cell Temperature
PV	Photovoltaic
STC	Standard Test Conditions (cell temp. 25 °C; irradiance 1000 W/m^2; air mass 1.5)

Greek Symbols

α_{Rs}	Series resistance temperature coefficient (linear law)

References

1. Rauschenbach, H.S. Solar Cell Array Design Handbook. In *The Principles and Technology of Photovoltaic Energy Conversion*; Springer: New York, NY, USA, 1980; pp. 167–183, ISBN 978-9401179171.
2. Patel, M.R. *Wind and Solar Power Systems*; CRC Press: Boca Raton, FL, USA, 1999; pp. 32–48, 137–157, ISBN 0-8493-1605-7.
3. Emery, K. Measurement and Characterization of Solar Cells and Modules. In *Handbook of Photovoltaic Science and Engineering*, 2nd ed.; Luque, A., Hegedus, S., Eds.; John Wiley & Sons: Hoboken, NJ, USA, 2011.
4. Aparicio, M.P.; Pelegrí-Sebastiá, J.; Sogorb, T.; Llario, V. Modeling of Photovoltaic Cell Using Free Software Application for Training and Design Circuit in Photovoltaic Solar Energy. In *New Developments in Renewable Energy*; Arman, H., Yuksel, I., Eds.; InTech: Vienna, Austria, 2013; pp. 121–139, ISBN 978-953-51-1040-8.

5. Sumathi, S.; Kumar, L.A.; Surekha, P. *Solar PV and Wind Energy Conversion Systems. An Introduction to Theory, Modeling with MATLAB/SIMULINK, and the Role of Soft Computing Techniques*; Springer: Cham, Switzerland, 2015; pp. 59–144, ISBN 978-3-319-14940-0.

6. Khatib, T.; Elmenreich, W. *Modeling of Photovoltaic Systems Using MATLAB: Simplified Green Codes*; John Wiley & Sons: Hoboken, NJ, USA, 2016; pp. 39–88. ISBN 978-1119118107.

7. Honsberg, C.; Bowden, S. Photovoltaic Education Network. Available online: http://pveducation.org/pvcdrom/instructions (accessed on 21 October 2017).

8. Van Zeghbroeck, B. Principles of Semiconductor Devices, 2011. Available online: https://ecee.colorado.edu/~bart/book/ (accessed on 21 October 2017).

9. LTSpice. Available online: http://www.linear.com/designtools/software/ (accessed on 21 October 2017).

10. Visual Studio Community. Available online: https://www.visualstudio.com/free-developer-offers/ (accessed on 21 October 2017).

11. S-Math Studio. Available online: https://en.smath.info/view/SMathStudio/summary/ (accessed on 21 October 2017).

12. Green, M.A. Solar cell fill factors: General graph and empirical expressions. *Solid State Electron.* **1981**, *24*, 788–789. [CrossRef]

13. Phang, J.C.H.; Chan, D.S.H.; Phillips, J.R. Accurate Analytical Method for the Extraction of Solar Cell Model Parameters. *Electron. Lett.* **1984**, *20*, 406–408. [CrossRef]

14. Liu, G.; Dunford, W.G. Photovoltaic Array Simulation. In Proceedings of the ESA Sessions at 16th Annual IEEE PESC, Universite Paul Sabatier, Toulouse, France, 24–28 June 1985; pp. 145–153.

15. Gow, J.A.; Manning, C.D. Development of a photovoltaic array model for use in power-electronics simulation studies. *IEE Proc.-Electr. Power Appl.* **1999**, *146*, 193–200. [CrossRef]

16. Walker, G. Evaluating MPPT converter topologies using a MATLAB PV model. *J. Electr. Electron. Eng.* **2001**, *21*, 49–55.

17. De Blas, M.A.; Torres, J.L.; Prieto, E.; Garcia, A. Selecting a suitable model for characterizing photovoltaic devices. *Renew. Energy* **2002**, *25*, 371–380. [CrossRef]

18. Xiao, W.; Dunford, W.G.; Capel, A. A Novel Modeling Method for Photovoltaic Cells. In Proceedings of the 35th Annual IEEE Power Electronics Specialists Conference, Aachen, Germany, 20–25 June 2004; pp. 1950–1956.

19. King, D.L.; Boyson, W.E.; Kratochvill, J.A. Photovoltaic Array Performance Model, Sandia National Laboratories. December 2004. Available online: http://prod.sandia.gov/techlib/access-control.cgi/2004/043535.pdf (accessed on 21 October 2017).

20. De Soto, W.; Klein, S.A.; Beckman, W.A. Improvement and validation of a model for photovoltaic array performance. *Sol. Energy* **2006**, *80*, 78–88. [CrossRef]

21. Schlosser, V.; Ghitas, A. Measurement of Silicon Solar Cells AC Parameters. In Proceedings of the Arab Regional Solar Energy Conference (ARSEC 2006), University of Bahrain, Zallaq Kingdom of Bahrain, 5–7 November 2006; pp. 1–15.

22. Villalva, M.G.; Gazoli, J.R.; Filho, E.R. Comprehensive Approach to Modeling and Simulation of Photovoltaic Arrays. *IEEE Trans. Power Electr.* **2009**, *24*, 1198–1208. [CrossRef]

23. Kim, S.K.; Jeon, J.H.; Cho, C.H.; Kim, E.S.; Ahn, J.B. Modeling and simulation of a grid-connected PV generation system for electromagnetic transient analysis. *Sol. Energy* **2009**, *83*, 664–678. [CrossRef]

24. Di Piazza, M.C.; Vitale, G. Photovoltaic field emulation including dynamic and partial shadow conditions. *Appl. Energy* **2010**, *87*, 814–823. [CrossRef]

25. Jung, J.H.; Ahmed, S. Model Construction of Single Crystalline Photovoltaic Panels for Real-time Simulation. In Proceedings of the IEEE Energy Conversion Congress and Exposition, Atlanta, GA, USA, 12–16 September 2010.

26. Kim, W.; Choi, W. A novel parameter extraction method for the one-diode solar cell model. *Sol. Energy* **2010**, *84*, 1008–1019. [CrossRef]

27. Ishaque, K.; Salam, Z. An improved modeling method to determine the model parameters of photovoltaic (PV) modules using differential evolution (DE). *Sol. Energy* **2011**, *85*, 2349–2359. [CrossRef]

28. Saloux, E.; Teyssedoua, A.; Mikhail, S. Explicit model of photovoltaic panels to determine voltages and currents at the maximum power point. *Sol. Energy* **2011**, *85*, 713–722. [CrossRef]

29. Cuce, P.M.; Cuce, E. A Novel model of photovoltaic modules for parameter estimation and thermodynamic assessment. *Int. J. Low Carbon Technol.* **2011**, *7*, 159–165. [CrossRef]

30. Tian, H.; Mancilla-David, F.; Ellis, K.; Muljadi, E.; Jenkins, P. A cell-to-module-to-array detailed model for photovoltaic panels. *Sol. Energy* **2012**, *86*, 2695–2706. [CrossRef]

31. Cubas, J.; Pindado, S.; de Manuel, C. Explicit Expressions for Solar Panel Equivalent Circuit Parameters Based on Analytical Formulation and the Lambert W-Function. *Energies* **2014**, *7*, 4098–4115. [CrossRef]

32. Aller, J.; Viola, J.; Quizhpi, F.; Restrepo, J.; Ginart, A.; Salazar, A. Implicit PV cell parameters estimation used in approximated closed-form model for inverter power control. In Proceedings of the 2017 IEEE Workshop on Power Electronics and Power Quality Applications (PEPQA), Bogotá, Colombia, 31 May–2 June 2017; pp. 1–6.

33. Chan, D.; Phang, J. Analytical Methods for the Extraction of Solar-Cell Single- and Double-Diode Model Parameters from I-V Characteristics. *IEEE Trans. Electron Devices* **1987**, *34*, 286–293. [CrossRef]

34. Sandrolini, L.; Artioli, M.; Reggiani, U. Numerical method for the extraction of photovoltaic module double-diode model parameters through cluster analysis. *Appl. Energy* **2010**, *87*, 442–451. [CrossRef]

35. Ishaque, K.; Salam, Z. A comprehensive MATLAB Simulink PV system simulator with partial shading capability based on two-diode model. *Sol. Energy* **2011**, *85*, 2217–2227. [CrossRef]

36. Soon, J.J.; Low, K.S.; Goh, S.T. Multi-dimension diode photovoltaic (PV) model for different PV cell technologies. In Proceedings of the IEEE 23rd International Symposium on Industrial Electronics (ISIE), Istanbul, Turkey, 1–4 June 2014; pp. 1–6.

37. Pandey, P.K.; Sandhu, K.S. Multi Diode Modelling of PV Cell. In Proceedings of the IEEE 6th India International Conference on Power Electronics (IICPE), Kurukshetra, India, 8–10 December 2014; pp. 1–4.

38. Erdem, Z.; Erdem, M.B. A Proposed Model of Photovoltaic Module in Matlab/SimulinkTM for Distance Education. *Procedia Soc. Behav. Sci.* **2013**, *103*, 55–62. [CrossRef]

39. 156 mm Monocrystalline Mono Solar Cell 6 x 6. Available online: https://www.aliexpress.com/item/50pcs-lot-4-6W-156mm-mono-solar-cells-6x6-150feet-Tabbing-Wire-15feet-Busbar-Wire-1pc/1932804007.html (accessed on 21 September 2017).

40. Radziemska, E.; Klugmann, E. Thermally affected parameters of the current–voltage characteristics of silicon photocell. *Energy Convers. Manag.* **2002**, *43*, 1889–1900. [CrossRef]

41. Tsuno, Y.; Hishikawa, Y.; Kurokawa, K. Temperature and Irradiance Dependence of the I–V Curves of Various Kinds of Solar Cells. In Proceedings of the 15th International Photovoltaic Science & Engineering Conference PVSEC-15, Shanghai China, 10–15 October 2005; pp. 422–423.

42. Singh, P.; Singh, S.N.; Lal, M.; Husain, M. Temperature dependence of I–V characteristics and performance parameters of silicon solar cell. *Sol. Energy Mater. Sol. Cells* **2008**, *92*, 1611–1616. [CrossRef]

43. Cuce, E.; Bali, T. Variation of cell parameters of a p-Si PV cell with different solar irradiances and cell temperatures in humid climates. In Proceedings of the 4th International Energy and Environment Symposium, Sharjah, United Arab Emirates, 19–23 April 2009.

44. Ghani, F.; Duke, M. Numerical determination of parasitic resistances of a solar cell using the Lambert W-function. *Sol. Energy* **2011**, *85*, 2386–2394. [CrossRef]

45. Romary, F.; Caldeira, A.; Jacques, S.; Schellmanns, A. Themal Modelling to Analyze the Effect of Cell temperature on PV Modules Energy Efficiency. In Proceedings of the 14th European Conference on Power Electronics and Applications (EPE 2011), Birmingham, UK, 30 August–1 September 2011.

46. Wen, C.; Fu, C.; Tang, J.; Liu, D.; Hu, S.; Xing, Z. The influence of environment temperatures on single crystalline and polycrystalline silicon solar cell performance. *Sci. China Phys. Mech. Astron.* **2012**, *55*, 235–241. [CrossRef]

47. Cuce, E.; Cuce, P.M.; Bali, T. An experimental analysis of illumination intensity and temperature dependency of photovoltaic cell parameters. *Appl. Energy* **2013**, *111*, 374–382. [CrossRef]

48. Bellia, A.H.; Ramdani, Y.; Moulay, F.; Medles, K. Irradiance and Temperature Impact on Photovoltaic Power By Design of Experiments. *Rev. Roum. Sci. Tech.-Ser. Electrotech.* **2013**, *58*, 284–294.

49. Araneo, R.; Grasselli, U.; Celozzi, S. Assessment of a practical model to estimate the cell temperature of a photovoltaic module. *Int. J. Energy Environ. Eng.* **2014**, *5*, 1–16. [CrossRef]

50. Chander, S.; Purohit, A.; Sharma, A.; Nehra, S.P.; Dhaka, M.S. A study on photovoltaic parameters of mono-crystalline silicon solar cell with cell temperature. *Energy Rep.* **2015**, *1*, 104–109. [CrossRef]

51. Aller, J.; Viola, J.; Quizhpi, F. Explicit Model of PV Cells considering Variations in Temperature and Solar Irradiance. In Proceedings of the 2016 ANDESCON, Arequipa, Peru, 19–21 October 2016; pp. 1–4.

52. Solar Cell Model. Available online: https://www.mathworks.com/help/physmod/elec/ref/solarcell.html (accessed on 10 August 2017).
53. Personal Webpage Prof. Dr. Marcelo Gradella Villalva. Available online: https://sites.google.com/site/mvillalva/pvmodel (accessed on 21 September 2017).
54. Górecki, K.; Krac, E. Measurements of thermal parameters of solar modules. *J. Phys. Conf. Ser.* **2016**, *709*, 1–6. [CrossRef]
55. Górecki, K.; Górecki, P.; Paduch, K. Modelling Solar Cells with Thermal Phenomena Taken into Account. *J. Phys. Conf. Ser.* **2014**, *494*, 1–8. [CrossRef]
56. Krac, E.; Górecki, K. Modelling characteristics of photovoltaic panels with thermal phenomena taken into account. *IOP Conf. Ser. Mater. Sci. Eng.* **2016**, *104*, 012013. [CrossRef]